THE REMARKABLE X-RAY JET IN THE QUASAR 4C 20.24

D.A. Schwartz[1], H.L. Marshall[2], J. Gelbord[2], E.S. Perlman[3], M. Georganopoulos[3], M. Birkinshaw[4], D. M. Worrall[4], J.E.J. Lovell[5], D.L. Jauncey[5], L. Godfrey[6], G.V. Bicknell[6], D.W. Murphy[7], and S. Jester[8]

[1]Harvard-Smithsonian Center for Astrophysics,60 Garden St., Cambridge, MA, 02138, USA
[2]Kavli Institute for Astrophysics and Space Research, Massachusetts Institute of Technology, 77 Massachusetts Avenue, Cambridge, MA 02139, USA
[3]Department of Physics, Joint Center for Astrophysics, University of Maryland-Baltimore County, 1000 Hilltop Circle, Baltimore, MD 21250, USA
[4]Department of Physics, University of Bristol, Tyndall Avenue, Bristol BS8 1TL, UK
[5]CSIRO Australia Telescope National Facility, PO Box 76, Epping NSW 1710, Australia
[6]Research School of Astronomy and Astrophysics, Australian National University, Cotter Road, Weston Creek, Canberra, ACT72611, Australia
[7]Jet Propulsion Laboratory, 4800 Oak Grove Drive, Pasadena, CA 91109, USA
[8]Fermi National Accelerator Laboratory, P.O. Box 500, Batavia, IL, 60510, USA

ABSTRACT

The Chandra X-ray telescope has observed a jet in 4C 20.24 (= PKS B1055+201) for which the de-projected length is inferred to be greater than 1 Mpc. The arcsec scale X-ray and 1.46 GHz jets initially follow the direction of the VLBA jet emanating N from the 0.2 mas core, but then curve to the NNW through a total change in angle of about 45 degrees. The 22 arcsec length of the jet gives us one of the best opportunities to study independent spatial elements, in order to infer how the magnetic field and relativistic beaming factor change with distance from the core. We find a constant Doppler factor of about 6, up until the radio structure bends through two 90 degree turns. The remarkable feature of this jet is that we detect extended X-ray emission of about 14 arcsec full width, symmetric about the jet. Furthermore, a similar extended X-ray feature extends to the south, where no radio or X-ray jet is visible, terminating just before the south radio lobe. At the redshift z=1.11 of this quasar, the extended X-ray emission has a luminosity 3E44 ergs per second, comparable to a luminous X-ray cluster. This system gives us a laboratory where we can observe both the jet, and the medium with which it is interacting.

Key words: jets; quasars; X-rays; 4C 20.24; PKS 1055+201.

1. INTRODUCTION

The FR II radio source 4C20.24 is identified as a quasar at redshift z=1.11 (Bolton, Kinman, & Wall, 1968). This quasar, which is also cataloged as PKS 1055+201, was observed by *Chandra* as part of a snapshot survey of radio jets (Marshall et al., 2005a). The survey, which is on-going, consists of 56 flat spectrum quasars, selected from two samples. One is by Murphy, Browne, & Perley (1993), of radio sources at declination angles above 0°, with core flux densities at 5 GHz greater than 1 Jy, and the other by Lovell (1997) of Parkes catalog sources below declination -20°, with core flux densities at 2.7 GHz greater than 0.34 Jy. From their radio maps, we selected sources with radio jets longer than 2″ and for which we expected that 5 ks *Chandra* observations would yield X-ray detections for objects having as large a ratio of X-ray to radio flux as was observed for the jet in PKS 0637-752 (Schwartz et al., 2000; Chartas et al., 2000).

Chandra obsid 4889 acquired 4.7 ks data in an initial survey of 4C 20.24. This gave a clear detection, showing an X-ray jet extended about 20″ along the radio jet to the north (Marshall et al., 2006). The X-ray flux was roughly 6.5 μJy, only about 20% of that predicted based on the radio emission. We proposed a longer followup *Chandra* observation, motivated by the angular extent in X-rays. The 21″ length could in principle be divided into 25 independent angular resolution elements, based on the 0.77″ full width half maximum (FWHM) response. This could allow a detailed study of the change of magnetic field and Doppler factor vs. distance from the quasar. At the redshift z=1.11, an angular size of 1″ corresponds to 8.24 kpc in the plane of the sky[1].

In this talk we will present some of the remarkable X-ray features revealed in the 31.6 ks *Chandra* obsid 5733. In

[1]We use a flat, accelerating cosmology, with H_0=71 km s^{-1} Mpc^{-1}, $\Omega_m = 0.27$, and $\Omega_\Lambda = 0.73$

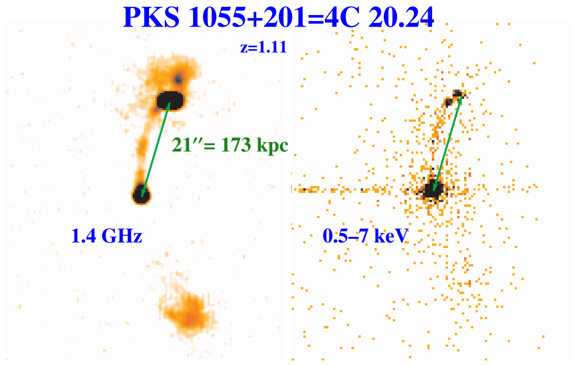

Figure 1. Left panel shows the 1.46 GHz radio image reconstructed with a 1.64″ × 1.5″ beam size, and the right panel the 0.5 – 7 keV X-ray image. The 21″ lines connect the same celestial coordinates in each panel. There is a clear X-ray jet to the north of the quasar, coincident with the radio jet, until the latter makes sharp bends to the west and then north. The horizontal feature on the X-ray image is the readout streak artifact. The X-ray image shows enhanced emission well beyond the width of the jet, and similar emission extending to the south.

particular, we detect extended X-ray emission surrounding the jet structure, and similar X-ray emission to the south surrounding an assumed, unseen counter-jet. In Section 2 we summarize some of the properties which 4C 20.24 shares in general with the other radio and X-ray jets we have studied, including the interpretation of the X-ray emission as inverse Compton (IC) scattering off the cosmic microwave background (CMB), (Tavecchio et al., 2000; Celotti et al., 2001). In Section 3 we present the unique X-ray features of this system. The final Section 4 discusses some possible mechanisms for the X-ray emission from the extended "tube" region.

2. WHAT IS NORMAL ABOUT THE 4C 20.24 JET?

In Fig. 1 we show the radio and X-ray images of 4C 20.24. The two images are to scale, and the double arrow is 21″ long which corresponds to 173 kpc in the plane of the sky. The arrow connects the same coordinates in each panel. The radio and X-ray jets are extremely similar, at least out to the point where the X-ray jet appears to end. In Fig. 1, the horizontal streak in the X-ray image is an artifact due to the fact that the ACIS CCD camera is not shuttered while a frame is being read out. Past the northern end of the arrow, the radio image appears to bend at nearly right angles to the west, and then again at a right angle to the north, where it terminates in a hotspot and lobe.

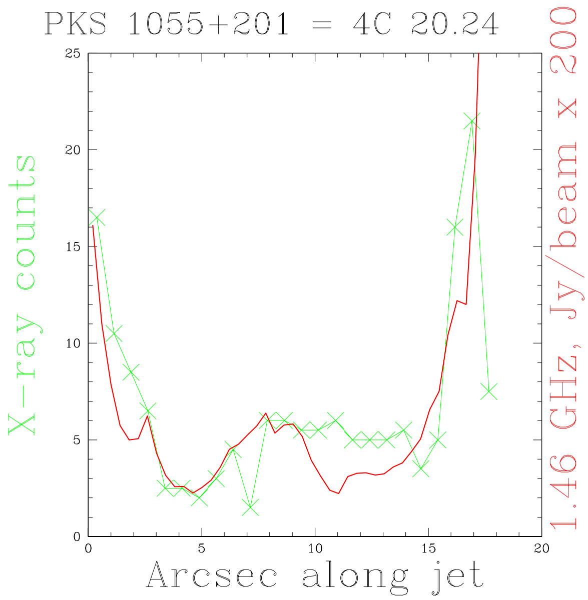

Figure 2. X-ray counts, crosses, sorted into 0.75″ bins, compared to the radio, solid line, 1.46 GHz flux density per beam, along a 4″ × 18″projection box. The X-ray counts have Poisson errors, but adjacent bins are correlated as the counts were split from the original 0.492″ bins. The radio flux density is arbitrarily multiplied by 200 to better compare to the X-ray profile.

2.1. Correlation to Radio emission

Fig. 2 compares the X-ray and radio profiles in more detail. Both images project identical areas of the sky, starting about 2″ from the quasar and extending 18″ along the jet; i.e., extending to where the radio emission bends toward the west. The projection is 4″ i.e., approximately ±2″ perpendicular to the jet. The crosses are the X-ray data, given in counts per bin.The heavier solid line is the 1.46GHz radio data. The radio emission in Jy/beam is multiplied by a factor of 200, to better compare to the X-ray profile. In Fig. 3 the radio data is given to the same scale of absolute physical units as the X-rays.

Over the range of 18″ corresponding to 148 kpc in the plane of the sky, the ratio of X-ray to radio flux does not change by more than a factor of 2. Since we infer from relativistic beaming that the jet is tilted no more than 9° from our line of sight, this would actually be a minimum distance of 948 kpc. In the range 2.5″ to 9.5″ the coincidence is even tighter. Such a similar ratio is hard to explain when the X-rays are due to either synchrotron or IC/CMB emission. In the synchrotron case both the radio and X-ray emission depend on the same magnetic field, but the lifetime of the X-ray emitting electrons is so short compared to the scale of the jet that a very fine tuned balance of high energy electron acceleration would be needed, and this acceleration must not simultaneously

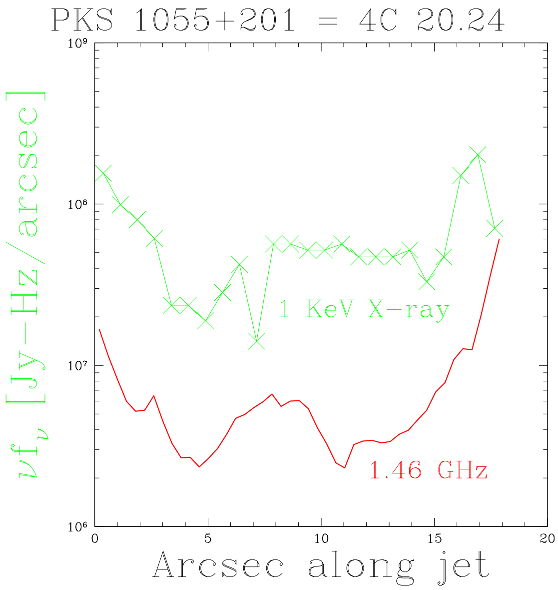

Figure 3. Both X-ray (crosses) and radio (solid line) are converted to absolute physical units of Jy-Hz arcsec^{-1} to show that the energy radiated in X-rays dominates over that radiated in the GHz band.

increase the number of longer lived radio emitting electrons. In the IC/CMB case, the X-rays result from electrons with lower energies than the radio, and both are longer lived than in the synchrotron case, but since the X-ray emission then does not depend on the magnetic field the latter would have to be finely tuned to be relatively constant. The naive prediction for IC/CMB would be for the X-ray emission to persist downstream of the radio emission, due to the longer life of the lower energy electrons, and we may be seeing this in the region around 10$''$ to 13$''$ along the jet. (The apparent X-ray dip at 7$''$ is not significant, due to the Poisson statistical errors.)

Fig. 3 plots νf_ν per arcsec along the jet. For the X-rays, we estimate a flux density at ν=2.4 $\times 10^{17}$ Hz, or 1 keV, by assuming an energy spectral index of α=0.7. The radio frequency is ν=1.46 GHz. We see the radiated energy in X-rays dominating that in radio by an order of magnitude, in the region shown. In contrast, the radio energy flux surpasses the X-ray beyond the terminal shocks, i.e., past the north end of the arrow in Fig. 1. In the sense that radio dominates X-ray at the end of the jet there is a similarity to the case of 3C 273, although for that object we see a constant decrease of the X-ray to radio ratio along the $\approx$10$''$ length of that jet.

2.2. Interpretation as Inverse Compton X-rays

Inverse Compton scattering of electrons by the cosmic microwave background photons (IC/CMB) has been widely inferred as the most plausible mechanism of X-ray emission from powerful, radio-loud quasars (Marshall et al., 2001; Sambruna et al., 2001, 2002, 2004; Harris & Krawczynski, 2002; Siemiginowska et al., 2002, 2003a,b; Schwartz et al., 2006) following the suggestion by Tavecchio et al. (2000) and Celotti et al. (2001) to explain the X-ray jet found in PKS 0637-752 (Schwartz et al., 2000; Chartas et al., 2000). Typically this is motivated by optical detection or upper limits which do not allow extrapolation of a single synchrotron spectrum from the radio to X-ray range. We will adopt the IC/CMB scenario here, although noting that other models have been constructed to try to produce the X-rays via synchrotron emission (e.g., Dermer & Atoyan (2002); Stawarz et al. (2004); Atoyan & Dermer (2004)).

We apply this formalism to the jet of 4C 20.24. We divide the X-ray jet into six distinct regions, each of 1.6$''$ radius, so that they enclose greater than 95% of the point spread function. The model assumes that the synchrotron emission arises from a region uniformly filled with a constant magnitude, randomly oriented magnetic field, and with minimum energy conditions between the particles and magnetic field. We assume an equal energy density of protons and electrons, and that the observed radio emission would extend over the range 10^6 Hz to 10^{12} Hz. This allows calculation of the magnetic field strength, B_1, required to generate the observed radio emission under the minimum energy condition. Such a magnetic field strength is typically much greater than the field one would calculate by assuming that the X-rays arise via IC/CMB from a volume at rest with respect to the CMB. However, Tavecchio et al. (2000) and Celotti et al. (2001) both pointed out that if the jet were in bulk relativistic motion with Lorentz factor Γ at an angle $\cos(\theta)$ to our line of sight, then in the rest frame of the jet the actual magnetic field would be $B=B_1/\delta$, where the Doppler factor $\delta = (\Gamma(1-\beta\cos(\theta))^{-1}$. Furthermore, the apparent CMB energy density seen by the photons in the jet is enhanced by a factor Γ^2 (Dermer & Schlickeiser, 1994). By assuming that $\Gamma = \delta$, which is the value of Γ for the maximum angle which can occur at any fixed δ we have only the two unknowns B and δ, which can then be estimated from the radio and X-ray flux densities.

Fig. 4 shows the results of this modeling. For the five innermost regions, labeled *a* through *e*, the magnetic fields are in the range 1 to 16 μGauss, and the Doppler factors in the range δ=5.5 to 6.5. Such values of δ imply that the angle to our line of sight cannot be greater than θ=9°. The values of B and δ are consistent with being constant, within the statistics of the X-ray counts, and especially due to the systematic uncertainties underlying the model assumptions. The final region, at the apparent terminal shock around the northern arrow point in Fig. 1, shows a significantly higher magnetic field and lower Doppler factor. This presumably is due to deceleration of the jet, and conversion of the bulk kinetic energy into magnetic field and relativistic particles. At 1.46 GHz, this region outshines the quasar by a factor of about three. However, it seems clear that the formalism is not self-consistent in interpreting both this region and the inner five regions. This can be seen by the deviation of point *f* from the solid line in Fig. 4. That line represents a constant kinetic energy flux, of about 3×10^{45} ergs s^{-1}, averaged over the

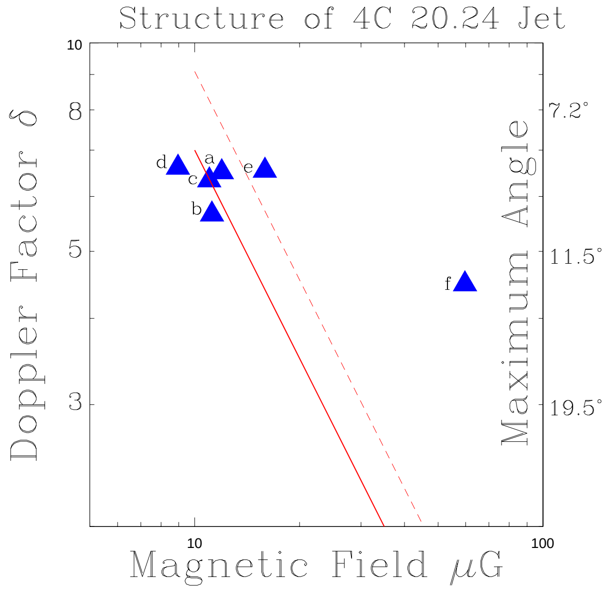

Figure 4. The effective Doppler factor and the magnetic field strength in the jet rest frame for six regions along the jet, labeled alphabetically away from the quasar. The solid line is the locus of kinetic luminosity 3×10^{45}*ergs* s^{-1} *of the five innermost regions, assuming equal proton and electron energy densities. The dashed line would represent the average of all six regions. The right hand scale shows the maximum possible angle at which the corresponding Doppler factor can be achieved. This occurs when* $\Gamma = \delta$.

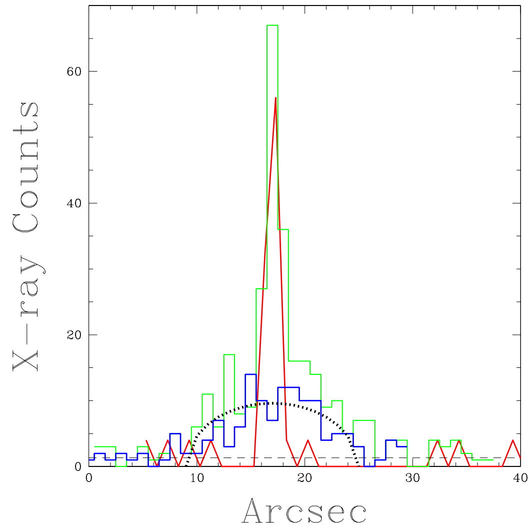

Figure 5. The two histograms show the X-ray profile along the jet (larger values, lighter line) and counter jet (smaller values, darker line) directions, plotted vs. angle across the jet. The continuous line is the scaled profile of the readout streak, which shows how an unresolved line source would appear. The dashed horizontal line shows the background level. The dotted profile is that expected from uniform emission of a cylinder.

five inner regions. The outermost region would require a minimum energy flux ten times greater. Possible solutions are that the kinetic flux is really about 3×10^{46} ergs s^{-1} through out the jet, e.g., due to a much greater proton to electron ratio than assumed or to conditions deviating from equipartition; or that the region f is at a non-relativistic velocity and not emitting X-rays via minimum energy IC/CMB.

3. WHAT IS REMARKABLE ABOUT THE 4C 20.24 JET?

4C 20.24 shows at least two remarkable features which have not previously been noted for FRII/quasar X-ray jets. One is the broad, about 16″ wide tube-like region of enhanced X-ray emission following the narrow X-ray and radio jet to the north and terminating at the same distance that the X-ray jet ends. The other is a similar symmetric feature to the south, following what might be assumed to be an unseen counter-jet.

Both tube regions appear to be curved to the west of the quasar. This can be substantiated; e.g., against the hypothesis that only one jet is deflected from an initial straight line, by considering the VLBI image. Kellerman et al. (2004) report six years of VLBA monitoring, where the core at 15 GHz is clearly extended by about 3 mas at position angle -5°. Within a few degrees uncertainty, this is the same initial angle that each of the radio and X-ray jet follows for the first few arcsecond north of the quasar.

An impression of the enhanced X-ray tubes can be seen directly in Fig. 1. A more quantitative result can be derived from Fig. 5. The figure presents two histograms which show the X-ray profile across the jet north and south of the core. These are constructed by integrating along 17″ lengths parallel to the jet and counter-jet directions. The horizontal dashed line close to zero counts represents the background measured in an identical projection in a nearby, source-free region. The continuous line results from a projection region that straddles the readout streak; it represents the width of an unresolved source and has been rescaled for comparison with the component of the northern histogram resulting from the projection of the narrow jet. Emission in each of the northern and southern regions extends at least from 10″ to 26″ in the plot, and hints at even broader extension which is fainter than the sensitivity of the present observation.

In the north and south regions of the X-ray tube, excluding the narrow jet, we have 310 X-ray counts. The spectrum of these counts allow a fit to a power law, with energy index α=0.66±0.2, Fig. 6. More complex models cannot be ruled out; for example, a power law with $\alpha=0.4^{+0.7}_{-3.3}$ plus a thermal spectrum with $kT=1.3^{+4.4}_{-1.2}$, Fig. 7. We include this latter model since it is relevant to discuss whether the X-ray tube emission arises from thermal bremsstrahlung. The X-ray spectrum of the jet can be fit with a power law of energy index α=0.98±0.25. Formally the two regions may therefore have the same spectrum; however, the spectrum of the narrow jet is somewhat softer than that of the tube. This can be seen simply from the integral distribution of photons in Fig. 8. A K-S test rejects these distributions being equal at the 99.95% confidence level. The spectral fit to the jet is based on 241 photons. However, from the profile of the extended X-rays, we can estimate that 40 of these are from the tube region projected in front and behind the jet and which has a harder spectrum, so that the residual jet spectrum will be even somewhat softer.

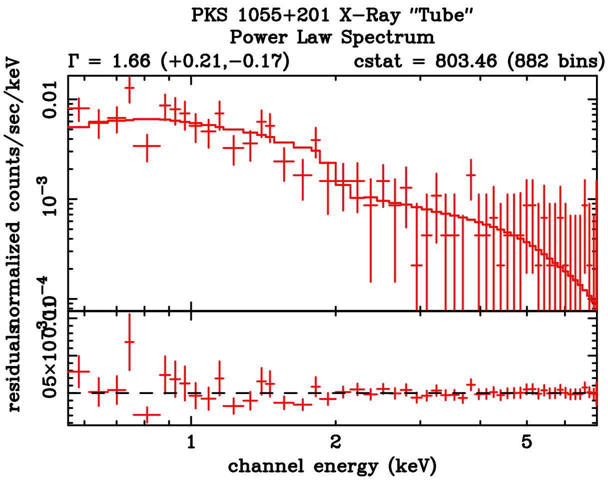

Figure 6. X-ray spectrum of the extended tube region, fit to a single power law. Residuals are shown in the bottom panel.

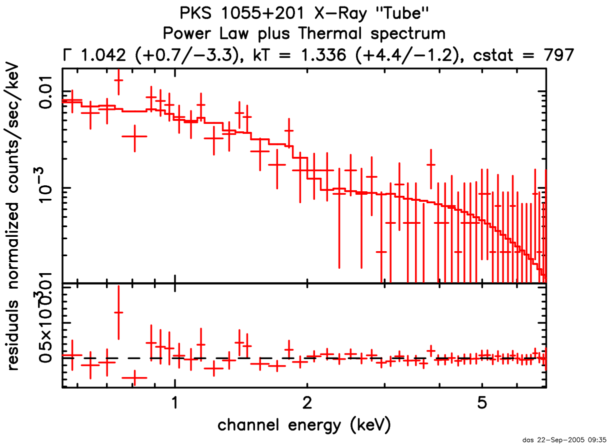

Figure 7. X-ray spectrum of the extended tube region, fit to the sum of a power law and a mekal thermal spectrum.

4. DISCUSSION

We discuss the extended X-ray tube in terms of thermal vs. non-thermal emission. Although a simple non-thermal power law is indicated by the X-ray spectrum, a

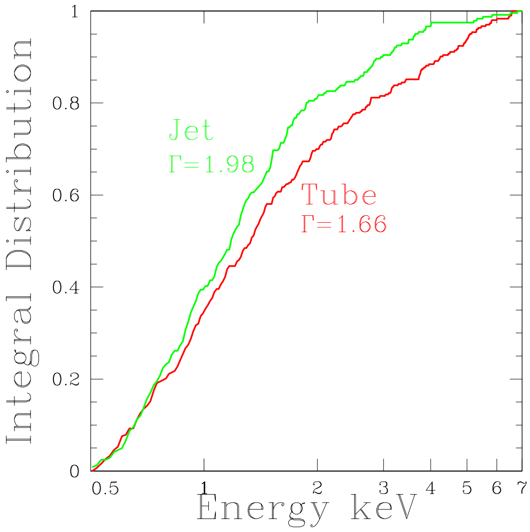

Figure 8. Integral distributions of the counts from the narrow jet and from the extended X-ray tube. The maximum absolute difference of 0.1317 at 1.9 keV shows that the two spectra cannot be identical, according to a two-tail K-S test.

thermal component cannot be strongly limited. In either case we model the tube as two uniformly filled cylinders, each of 65 kpc radius and 1 Mpc in length. The dotted curve in Fig. 5 shows the expected projection of such an emission region. The numbers here may be rough, pending more detailed spectral and spatial analysis.

From the fit to a thermal mekal model plus a power law, the thermal normalization implies an X-ray luminosity of 2.5×10^{44}ergs s^{-1} emitted in the 1 to 15 keV band in the source frame. We note that this would be grossly overluminous if it were thought to arise in a cluster of galaxies with such a low temperature kT=1.34 keV. At that gas temperature, the density would be n_e=0.0054 cm^{-3} to produce the luminosity. The total energy content of the gas would be of order 10^{61} ergs, requiring our estimated kinetic flux of 3 $\times10^{45}$ ergs s^{-1} to be maintained for $\approx 10^8$ years and to be efficiently converted into heating the gas. However, the cooling time scale of the gas is of order 4×10^9 years, so that it is conceivable that several different epochs of radio-activity could contribute to the thermal reservoir. Gas at such a cool temperature will show a very strong complex of Fe-L line emission, observable in the 0.45 to 0.55 keV range. With of order ten times as many X-ray photons, one should be able to observe a temperature gradient whose hot end would point to the location of interaction. The jet energy might be dissipated laterally, e.g., through entrainment of material or lateral shocks. However, since we do not see evidence for deceleration out to at least 17′′ from the quasar, the dissipation may be taking place at the terminal shock. In this case the base of the tubes, nearest the quasar, would show the coolest temperatures. The mass of gas required to fill the cylinders in the thermal scenario is of order 2 ×

10^{12} solar masses.

Non-thermal emission allows many scenarios for the origin of the relativistic electrons. We consider a case where the electrons diffuse out of the jet and into a region of low magnetic field which is not in bulk relativistic motion with respect to the microwave background. In this case the entire X-ray emission is produced by IC/CMB, giving an X-ray luminosity of 5.4×10^{44} ergs s^{-1}. The required density of relativistic electrons is of order 3×10^{-8} cm^{-3}, comparable to the density in the jet. Their lifetime against IC/CMB emission is of order 10^8 years, so a diffusion velocity of $\approx$ 300 km s^{-1} would be required to propagate 65 kpc away from the jet. This scenario gives a clear prediction of low frequency radio emission. Since we may still conjecture magnetic fields of order 0.1 to 1 μGauss we may detect the tube region in the few 100 MHz range. We should see a steeper X-ray spectrum laterally away from the jet, at distances comparable to the electron lifetimes. Alternately, if the relativistic electrons are back-streaming from the terminal hotspot, the steeper spectra will be toward the base of the jet.

4C 20.24 gives us an opportune system for deducing the spatial structure of the magnetic fields and Doppler factors in an X-ray/radio jet. The relativistic beaming IC/CMB scenario can explain the X-ray and radio emission along the length of the jet, but we require a scenario with non-relativistic motion to explain the terminal shock. The extended X-ray emitting "tubes" surrounding this jet are unique. There are problems explaining them as either thermal gas, or electrons diffusing out of the jet. The situation requires a much deeper X-ray image to further elucidate the spatial emission profile and the spatially dependent spectral shape, and low frequency radio observations. In any event, the southern X-ray structure provides new evidence for the presence of unseen counter jets, which hitherto have been inferred by the presence of radio lobes.

ACKNOWLEDGMENTS

This work was supported by NASA contract NAS8-39073 to the *Chandra* X-ray Center, and SAO SV1-61010 to MIT, and NASA grant GO2-3151C to SAO. E.S.P. acknowledges support from NASA LTSA grant NAG5-9997. Part of this research was performed at the Jet Propulsion Laboratory, California Institute of Technology, under contract to NASA. This research used the NASA Astrophysics Data System Bibliographic Services, and the NASA/IPAC Extragalactic Database (NED) which is operated by the Jet Propulsion Laboratory, California Institute of Technology, under contract with the National Aeronautics and Space Administration.

REFERENCES

Atoyan, A. & Dermer, C. D. 2004, ApJ, 613, 151

Bolton, J. G., Kinman, T. D., & Wall, J. V. 1968, ApJ, 154, L105

Celotti, A., Ghisellini, G., & Chiaberge, M. 2001, MNRAS, 321, L1

Chartas, G., et al. 2000, ApJ, 542, 655

Dermer, C. D. & Atoyan, A. M. 2002, ApJ, 568, L81

Dermer, C. D. & Schlickeiser, R. 1994, ApJS, 90, 945

Harris, D. E., & Krawczynski, H. 2002, ApJ, 565, 244

Kellerman, K. I. et al. 2004, ApJ, 609, 539

Lovell, J. 1997, Ph.D. Thesis, U. of Tasmania

Marshall, H. L., et al. 2001, ApJ, 549 L167

Marshall, H. L., et al. 2005a, ApJS, 156, 13

Marshall, H. L., et al. 2006, in preparation

Murphy, D.W., Browne, I.W.A., & Perley, R.A. 1993, MNRAS, 264, 298

Sambruna, R.M., Urry,C.M. Tavecchio, F., Maraschi, L., Scarpa, R., Chartas, G., & Muxlow,T. 2001, ApJ, 549, L161

Sambruna, R. M., Maraschi, L., Tavecchio, F., Urry, C. M., Cheung, C. C., Chartas, G., Scarpa, R., & Gambill, J. K. 2002, ApJ, 571, 206

Sambruna, R. M., Gambill, J.K., Maraschi, L., Tavecchio, F., Cerutti, R., Cheung, C. C., Urry, C. M., & Chartas, G., 2004, ApJ, 608, 698

Schwartz, D. A., et al. 2000,ApJ, 540, L69

Schwartz, D. A., et al. 2006, ApJ, in press

Siemiginowska, A, Bechtold, J., Aldcroft, T. L., Elvis, M., Harris, D. E., Dobrzycki, A. 2002, ApJ, 570, 543

Siemiginowska, A., et al. 2003a, ApJ, 595, 643

Siemiginowska, A., Smith, R. K., Aldcroft, T. L., Schwartz, D. A., Paerels, F., & Petric, A. O. 2003b, ApJ, 598, L15

Stawarz, Ł., Sikora, M., Ostrowski, M., & Begelman, M. C. 2004, ApJ, 608, 95

Tavecchio, F., Maraschi, L., Sambruna, R. M., Urry, C. M. 2000, ApJ, 544, L23